Article

Spectroscopic and Physicochemical Studies on 1,2,4-Triazine Derivative

Arwa Alrooqi [1,2], Zahra M. Al-Amshany [1], Laila M. Al-Harbi [1] , Tariq A. Altalhi [3,*] , Moamen S. Refat [3] ,
Ali M. Hassanien [4] , Gaber A. M. Mersal [3] and Ahmed A. Atta [5]

1 Department of Chemistry, Faculty of Sciences, King Abdulaziz University, P.O. Box 80203,
Jeddah 21589, Saudi Arabia; asalemalroge@stu.kau.edu.sa (A.A.); zalamshany@kau.edu.sa (Z.M.A.-A.);
lalhrbi@kau.edu.sa (L.M.A.-H.)
2 Department of Chemistry, Faculty of Arts and Science, Al-Baha University, P.O. Box 1988,
Baljurashi 65634, Saudi Arabia
3 Department of Chemistry, College of Science, Taif University, P.O. Box 11099, Taif 21944, Saudi Arabia;
moamen@tu.edu.sa (M.S.R.); gamersal@yahoo.com (G.A.M.M.)
4 Department of Physics, College of Science and Humanities, Shaqra University, P.O. Box 1040,
Al Quwaiiyah 11971, Saudi Arabia; ahassanien@su.edu.sa
5 Department of Physics, College of Science, Taif University, P.O. Box 11099, Taif 21944, Saudi Arabia;
a.atta@tu.edu.sa
* Correspondence: ta.altalhi@tu.edu.sa or tmmba@windowslive.com

Abstract: A novel 5-(5-Bromo-2-hydroxybenzylidene)-6-oxo-3-phenyl-5,6-dihydro-1,2,4-triazine-2(1H)-carbothioamide (4) "**compound 4**" was synthesized. The chemical structure of **compound 4** was confirmed with spectroscopic techniques. Thermal analysis (TGA/dTGA) studies were conducted for identifying the kinetic thermodynamic parameters and the thermal stability of the synthesized **compound 4.** Cyclic voltammetric studies were performed for recognizing electrochemical characteristics of the synthesized **compound 4.** The calculated highest occupied molecular orbital (HOMO), lowest unoccupied molecular orbital (LUMO), and the band gap were found to be −3.61, −5.32, and 1.97 eV, respectively. Using a diffused reflectance spectroscopy (DRS) technique, the estimated values of the optical band transitions of **compound 4** in powder form were found to be 2.07 and 2.67 eV. The structural properties of thermally evaporated **compound 4** thin films were analyzed using field emission scanning electron microscopy (FESEM), X-ray diffraction (XRD), and Fourier transform infrared (FTIR) spectroscopy. It was found that **compound 4** has a triclinic crystal structure. The optical transitions and the optical dispersion factors of **compound 4** thin films were investigated using a UV-Vis spectroscopy technique. From the UV-Vis spectroscopy technique, $E_g^{ind} = 3.6\,V$ was estimated for both the as-deposited and annealed thin films. For the as-deposited film, there were two photoluminescence (PL) emission peaks centered at 473 and 490 nm with a shoulder at 422 nm. For the annealed film at 423 K, there were five PL emission peaks centered at 274, 416, 439, 464, and 707 nm with a shoulder at 548 nm. The dark electrical conduction of **compound 4** thin film was through a thermally activated process with activation energy equaling 0.88 eV.

Keywords: organic thin films; electrochemical properties; structural properties; spectroscopic studies

1. Introduction

Small molecules of organic compounds are rapidly growing topics of electronic engineering and materials science that have led to the growth of light-harvesting and organic semiconducting materials with an extensive collection of properties and modern applications. The progress of new small molecules of organic compounds has been of great importance, owing to their extensive applications in optoelectronics, bio-imaging, and optical storage. Electronic devices based on organic compounds are at the head of current scientific research, with the goal of producing more environmentally efficient electronic devices. Organic materials can attain this, as they characteristically produce materials

that are less toxic and less solution-processable than their inorganic counterparts [1–14]. Electrochromic organic molecules have distinctive color-altering properties after passing an electrical current, making them extremely suitable for colored displays and smart windows [15–17]. To efficiently improve the luminescence properties of organic molecules for a certain optical wavelength region, the length of the conjugation is typically modified. In addition, the presence of both electron substituents accepting (A) and donating (D) in a single molecule shows remarkable optical properties owing to intramolecular charge transfer (ICT). This chemical phenomenon has remarkable applications in optoelectronics and nonlinear optical devices [18–20].

Organic semiconductors as active materials in thin-film electronic devices, such as alkenes, heterocycles, dyes, ferrocenes, spiranes, or porphyrins, with special geometries and some electronic molecular parameters that possess nonlinear optical (NLO) properties present several main advantages over their inorganic counterparts.

The recent literature has highlighted the growing interest in organic materials in recent decades as an alternative to inorganic analogs, and they have many advantages, such as low cost, low toxicity, ease of solution-handling, flexibility in device fabrication [21], and modifications of optical, electronic, and chemical properties through adapting molecular structure. Organic field-effect transistors (OFETs), organic solar cells (OSCs), and organic light-emitting diodes (OLEDs) are some of the applications of organic materials [22].

The deposition of organic materials in thin films, which is essential for designing new and successful devices, requires careful monitoring of their chemical, structural, and morphological properties [23]. The deposition of organic materials on thin films must meet market requirements: (1) good uniformity of simple or multilayer structures of organic, polymeric, or composite materials (in the electronics industry); (2) thickness control and coating uniformity; and (3) matching coatings required to modify the internal surfaces of porous materials (membranes, foams, or textiles) or irregular surface geometries (for medical and optoelectronic devices) [24].

Several articles have reported the synthesis of novel organic molecules or polymers with highly reactive chromophores and ultra-optical activity as a response to the demand for materials with NLO properties that can be used in various fields, such as modern applications, improving human life, and environmental remediation [21–41].

Novel organic conjugated compounds with remarkable electronic and optical characteristics have been investigated extensively in biological fluorescent probes, OFETs, OLEDs, and OSCs [21–24]. Heterocyclic compounds containing nitrogen atoms have exhibited electroluminescence and photoluminescence characteristics. Fused 1,2,4-triazine aromatic rings have been used as raw organic material for optoelectronic devices. Triazines are good electron-acceptor organic compounds that have been used as electron transport layers in OLEDs [25–27]. The modification of triazine rings by various substituents at different positions is promising for the development of new organic devices [42,43].
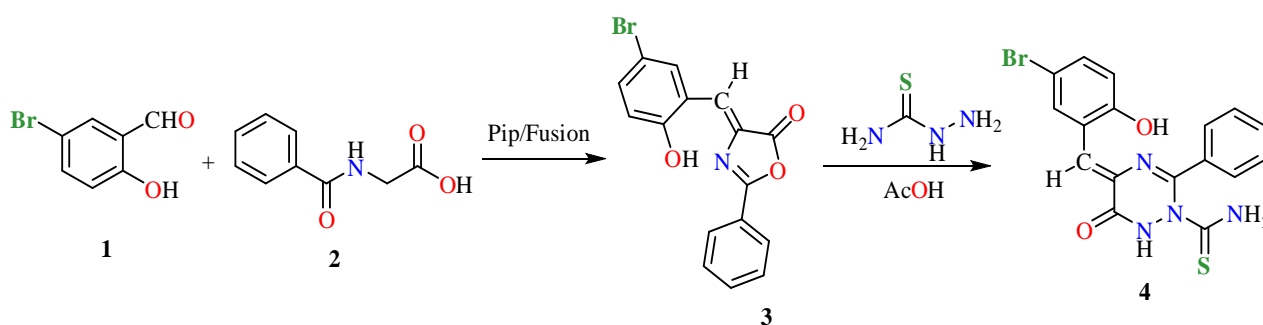
We investigate the physicochemical characteristics of small molecules of organic compounds in a solid state, where we essentially focus on thin films with regard to their applications in novel optoelectronic devices. This report focuses on the synthesis of a novel 5-(5-Bromo-2-hydroxybenzylidene)-6-oxo-3-phenyl-5,6-dihydro-1,2,4-triazine-2(1H)-carbothioamide (4) compound. In addition, the structural, electrochemical, spectroscopic, and physicochemical studies on this novel organic material in powder and thin-film forms are investigated.

2. Methods and Materials

Preparation of "5-(5-Bromo-2-hydroxybenzylidene)-6-oxo-3-phenyl-5,6-dihydro-1,2,4-triazine-2(1H)-carbothioamide" (4)

The used chemicals and solvents were purchased from Sigma Aldrich Chemical Company. The chemicals and solvents were AR-grade and were used without further purification required by standard methods. The synthesized compound (4) was passed through the sequence steps mentioned in Scheme 1: firstly, 5-bromosalicylaldehyde (Sigma

Aldrich, 98%, Merck KGaA, Darmstadt, Germany) **1** (2.01 g, 0.01 mol) and hippuric acid (Sigma Aldrich, 98%) **2** (1.79 g, 0.01 mol) were fused for about 1 hr in the presence of a few drops of piperidine (Sigma Aldrich, 99%) as a catalytic. The yellow solid product associated with the first step was recrystallized in ethanol to yield compound **3**. An amount of 3.44 g of compound **3** (0.01 mol) was dissolved in 20 mL glacial acetic acid (Sigma Aldrich), thiosemicarbazide (Sigma Aldrich, 99%) (0.91 gm, 0.01 mol) was added, and the total mixture was refluxed for 4 hrs (the progress of the reaction was monitored by TLC). The excess solvent was evaporated under a vacuum for collection, and then the solid product was crystallized in situ with ethanol (Sigma Aldrich) to yield orange crystals. **Compound 4** was synthesized in good yield (78 %) with an m.p. of 243–245 °C. It is soluble in ethanol, methanol, and common organic solvents, such as DMSO and DMF, but insoluble in chloroform, dichloromethane, carbon tetrachloride, and diethyl ether. The Anal. Calcd for $C_{17}H_{13}BrN_4O_2S$ (417.28) included: Calcd—C, 48.93; H, 3.14; Br, 19.15; N, 13.43; S, 7.68; Found—C, 48.65; H, 3.08; Br, 19.09; N, 13.31; S, 7.64.

Scheme 1. Preparation of "5-(5-Bromo-2-hydroxybenzylidene)-6-oxo-3-phenyl-5,6-dihydro-1,2,4-triazine-2(1H)-carbothioamide" (**4**).

The ^{1}H-NMR spectra were recorded on a JEOL 500 MHz spectrometer. The Fourier transform infrared spectroscopy (FT-IR) spectra were recorded using an ATR-FTIR spectrometer (Bruker, Pragsdorf, Germany) with a wavelength range from 400 to 4000 cm^{-1}. The scanning range was set from 4000 to 400 cm^{-1} with a scanning resolution of 4 cm^{-1} and 64 scans per sample using OPUS 6.0 suite (Bruker) software.

TGA and dTG thermograms were obtained in the temperature range of 20–800 °C with a heating rate of 10 °C min^{-1} in a nitrogen atmosphere using a Shimadzu (TGA-50H) thermal analyzer.

An Autolab potentiostat PGSTAT 302 (Eco Chemie, Utrecht, The Netherlands) with general-purpose electrochemical systems data processing software was used to investigate the electrochemical impedance spectroscopy (EIS) and cyclic voltammetry (CV) characteristics. Ag/AgCl was used as a reference electrode, and a carbon paste electrode was used as a working electrode, while a platinum wire was used as a counter electrode. The pH values were modified using a solution of 1 M NaOH. A Metrohm pH meter with a combined glass electrode was used to calculate the pH values. A USB4000-XR1-ES Ocean spectrometer (Ocean Insight, Orlando, FL, USA) was used to study the optical diffuse reflectance of **compound 4** in powder form. A Leybold Univex 300 thermal vacuum-coating apparatus (Leybold GmbH, Köln, Germany) was used to obtain thin films of **compound 4**. A vacuum of $\approx 7 \times 10^{-5}$ mbar was maintained through the thermal deposition process. At nearly 300 K, 300 nm of **compound 4** was deposited onto glass substrates at a rate of 0.1 nm/sec. XRD patterns were measured for **compound 4** using an X-ray diffractometer (Bruker, Billerica, MA, USA) with Cu K$_\alpha$. Field emission scanning electron microscope images (Hillsboro, OR, USA) were obtained with an SEM Quanta 250 FEG attached to an energy-dispersive X-ray unit. A spectrofluorometer (JASCO FP-8200, Jasco International Co. Ltd., Tokyo, Japan) was used to obtain room-temperature PL emission spectra of the **compound 4** thin films. The optical reflection and transmission spectra of the **compound 4** thin films were obtained using a UV-Vis double-beam UVD-3500 spectrophotometer (LABOMED INC,

Los Angeles, CA, USA) in the wavelength range of 190–900 nm at room temperature. A two-probe technique was used to measure dark DC electrical conductivity using a Keithley 6517 A high internal impedance electrometer (Keithley Instruments, Cleveland, OH, USA).

3. Results and Discussion

3.1. H-NMR and ^{13}C-NMR Spectral Studies

Figure 1 refers to the suggested structure of **compound 4** with atom numbering. Figures 2 and 3 display the ^{1}H- and ^{13}C-NMR spectra of **compound 4**. The ^{1}H- and ^{13}C-NMR spectral assignments of **compound 4** were as follows:
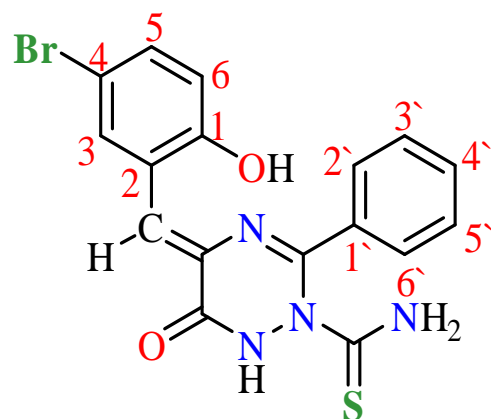
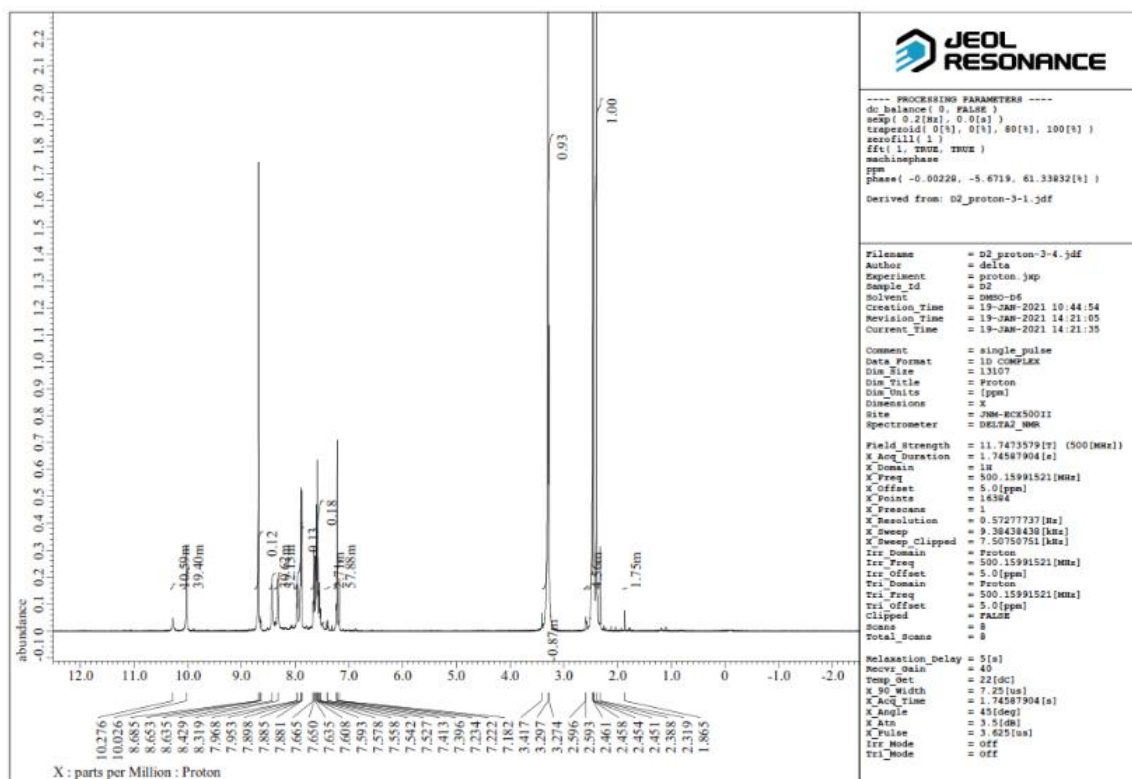

Figure 1. Numerical structure of **compound 4**.

Figure 2. ^{1}H-NMR of **compound 4**.

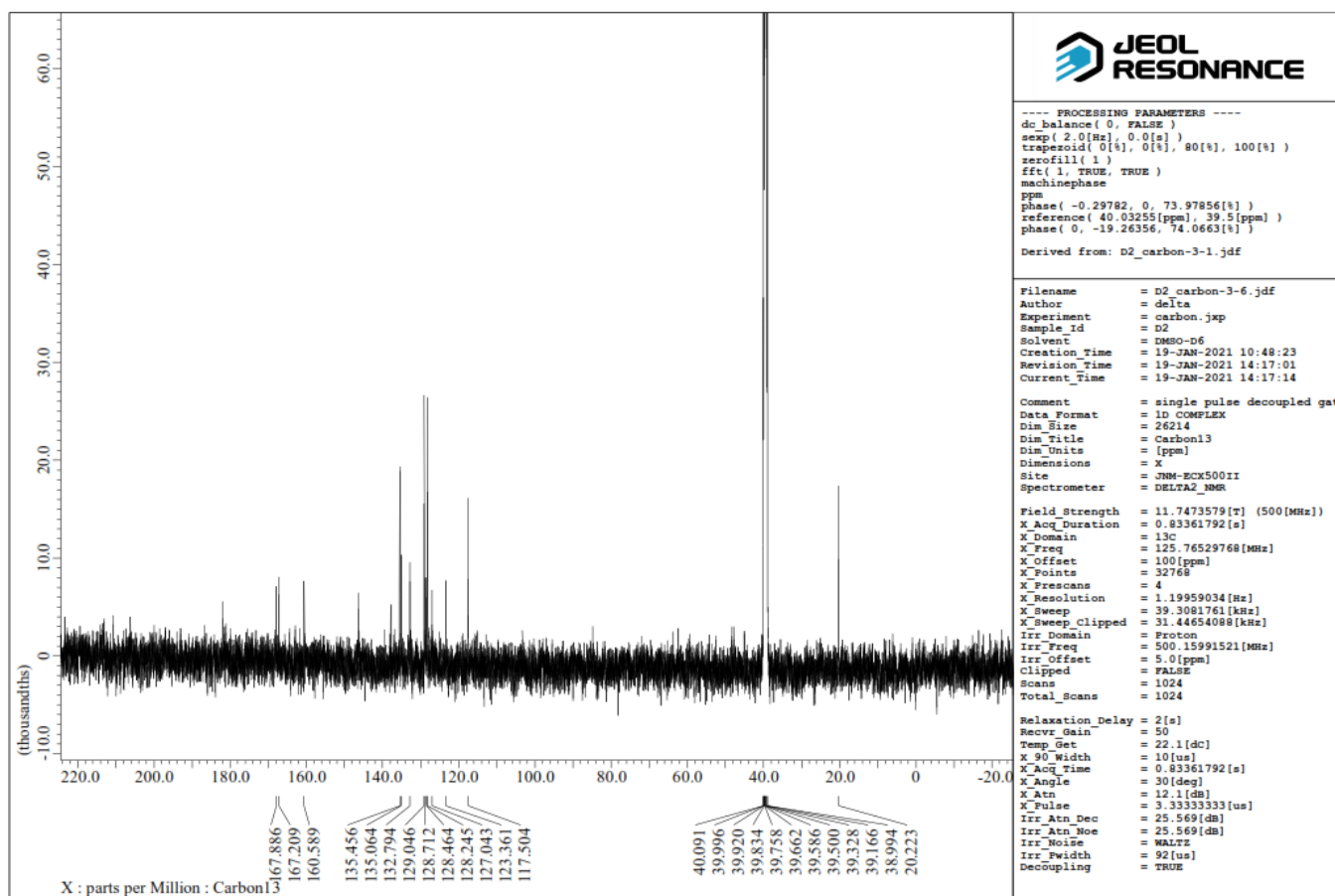**Figure 3.** ^{13}C-NMR of **compound 4**.

^{1}H-NMR (DMSO-d_6, 500 Mz): δ = 7.18 (s, 1H, CH=); 7.22 (s, 2H, NH_2); 7.39 (d, 1H, J = 8.5 Hz, C_6H); 7.52 (d, 1H, J = 7.5 Hz, C_5H); 7.55 (t, 2H, J = 10.0 Hz, $C_{1',6'}H$); 7.60 (t, 1H, J = 13.5 Hz, $C_{4'}H$); 7.88 (s, 1H, C_3H); 7.89 (m, 2H, $C_{3',5'}H$); 8.68 (s, 1H, OH); and 10.02 (s,1H, NH). ^{13}C-NMR (DMSO- d_6, 125Mz): δ = 117.5 C_4; 123.3 C_6; 127.0 C_2; 128.2 C_3; 128.4 $C_{2',6'}$; 128.7 $C_{3',5'}$; 129.0 $C_{4'}$; 132.7 HC = C; 135.0 C_5; 135.4 $C_{1'}$; 139.2 HC = C; 142.5 C_1; 160.5 C_3 triazine; 167.2 (C=O); and 181.2 (C=S).

3.2. Thermal Analysis Study

Figure 4 refers to the thermogravimetric curves and their differential for the synthesized **compound 4**. In the temperature range of 473–573 K (dTG curve), the total weight loss was found to be 65%, leaving more than 35% residue. The thermal decomposition of **compound 4** had only one step. This means that **compound 4** was thermally stable up to 473 K, and then it started to decompose until it reached 1073 K. The endothermic decomposition stage was assigned to the loss of most organic moieties with the remaining black un-oxidizing carbon atoms as a residual product.
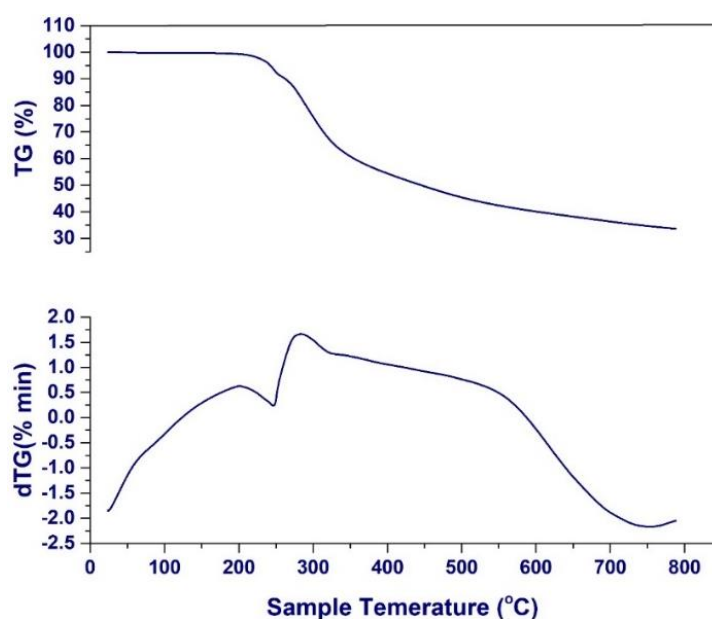
Figure 4. Thermal analysis (TGA/dTGA) of **compound 4**.

3.3. Kinetic Thermodynamic Parameter Calculations

A Coats–Redfern equation [44] was used to calculate the activation energy (E_a) of the decomposition step. The following equation was used for reaction order $ń \neq 1$:

$$log\left[\frac{1-(1- á)^{n-1}}{T^2(1-ń)}\right] = log\frac{ZŔ}{qE_a}\left[1-\frac{2ŔT}{E_a}\right] - \frac{E_a}{2.303ŔT} \quad for\ ń \neq 1 \tag{1}$$

$$log\left[\frac{-\log(1-á)}{T^2}\right] = log\frac{ZŔ}{qE_a}\left[1-\frac{2ŔT}{E_a}\right] - \frac{E_a}{2.303ŔT} \quad for\ ń = 1 \tag{2}$$

where $á$ is the fraction of weight loss, T is the temperature (K), $ń$ is the order of the reaction, Z is the pre-exponential factor, $Ŕ$ is the molar gas constant, E_a is the activation energy, and q is the heating rate. The activation energies (E_a) were calculated from the slopes of the best-fit straight lines ($r \approx 1$) obtained from the plots of the Coats–Redfern equation [44].

The kinetic thermodynamic parameters of entropy change (ΔS^*), enthalpy change (ΔH^*), and free energy of activation change (ΔG^*) were determined using the following equations:

$$\Delta S^* = Ŕ\ ln\left(\frac{Zh}{k_B T_s}\right) \tag{3}$$

$$\Delta H^* = E_a - Ŕ\ T \tag{4}$$

$$\Delta G^* = \Delta H^* - T\ \Delta S^* \tag{5}$$

where Z, k_B, and h are the pre-exponential factor, Boltzmann constant, and Plank constant, respectively [45]. T_s is the peak temperature of the derivative thermogravimetry (dTG). The kinetic thermodynamic parameters E_a, ΔH^*, ΔS^*, and ΔG^* were evaluated using the Coats–Redfern equation and are listed in Table 1. The activation entropy ΔS^* indicated that the activated compound has a more ordered structure than the reactants. The value of ΔG^* was positive, and ΔS^* was negative; these were considered unfavorable or non-spontaneous (thermally stable) reactions.

Table 1. Kinetic parameters of Coats–Redfern (CR) equation for **compound 4**.

r	$\acute{n}$	Z s^{-1}	T_{max} K	E_a KJ/mol^{-1}	ΔS^* J.k^{-1}·mol^{-1}	ΔH^* KJ/mol^{-1}	ΔG^* KJ/mol^{-1}
0.9998	0.8	3.65×10^6	527	132	−125	128	191

r is the correlation coefficient of the linear plot.

3.4. Cyclic Voltammetric Studies

The electrochemical behavior for **compound 4** was investigated using cyclic voltammetry (CV) in dichloromethane in the presence of 0.1 M tetrabutylammonium perchlorate (TBAP) using Pt wire as a working electrode and a 50 mV/s scan rate. Figure 5a shows the cyclic voltammogram for the Pt electrode in the absence of **compound 4**: no reduction or oxidation peaks appeared. Figure 5b shows the obtained voltammograms in the presence of **compound 4**: two quasireversible redox systems were obtained. For the first redox system, the oxidation peak (E_{pa1}) appeared at −0.52 V, while the cathodic peak (E_{pc1}) appeared at −0.93 V. The separation of the anodic and cathodic peak potentials (ΔE), which demonstrates the reversibility behavior of the reaction, was found at 0.41 V. The formal potential $E_{1/2}$, taken as the average of E_{pc1} and E_{pa1}, was −0.725 V. In the second redox system, the oxidation peak (E_{pa2}) appeared at + 0.123 V, while the cathodic peak (E_{pc2}) appeared at +0.643 V. The separation of the anodic and cathodic peak potentials (ΔE) was found as 0.59 V. The formal potential $E_{1/2}$ was taken as the average of E_{pc1} and E_{pa1} to be +0.935 V.
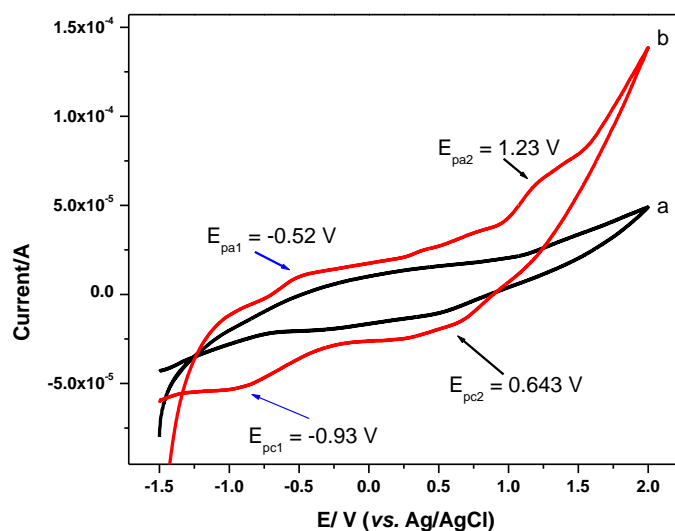

Figure 5. Cyclic voltammograms for Pt electrode in (**a**) the absence of **compound 4** and (**b**) the presence of **compound 4** in dichloromethane with 0.1 M TBAP using a 50 mV/s scan rate.

From the cyclic voltammetry technique, the band gap (E_g), which was calculated using the difference between the electrochemical HOMO and LUMO obtained, was calculated using the following equations [45–47]:

$$E_{HOMO} = -(E_{onset\,(oxidation)} + 4.4)\ eV \tag{6}$$

$$E_{LUMO} = -(E_{onset\,(reduction)} + 4.4)\ eV \tag{7}$$

The onsets of the oxidation $E_{(onset\,oxidation)}$ and reduction $E_{(onset\,reduction)}$ peaks were −0.79 V and +1.18 V, respectively. The calculated HOMO, LUMO, and the band gap ($E_g^{electrochemical}$) were found to be 3.61 eV, −5.32 eV, and 1.97 eV respectively. Altalhi et al. [48] estimated the $E_g^{electrochemical}$ of 4-amino-3-mercapto-6-(2-(2-thienyl)vinyl)-1,2,4-triazin-5(4H)-one donor to be 2.06 eV.

The effect of repetitive cycles on the peak currents of **compound 4** using cyclic voltammetry was examined by following the scan for cycles, as represented in Figure 6. By repeating the cyclic voltammograms, no matched effect was observed. This indicates that there was no absorption from **compound 4** of the electrode surface, and the electrode was relatively stable in dichloromethane solution.
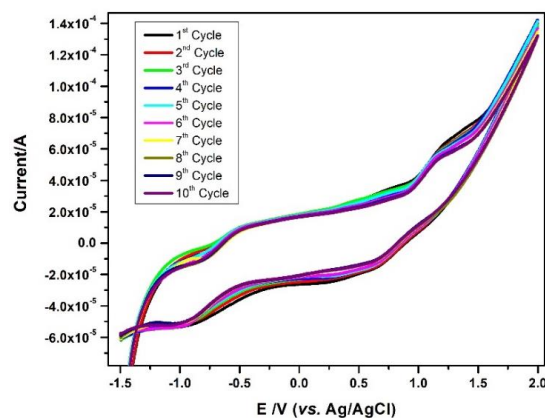

Figure 6. The effect of repetitive cycles on the peak currents of **compound 4**.

The effect of the scan rate was examined using a wide scan range, from 10 to 200 mV/s, as shown in Figure 7a. As shown in Figure 7b, by increasing the scan rate values, the oxidation and reduction peak currents increased. This behavior was expected for a diffusion-controlled electron transfer process.
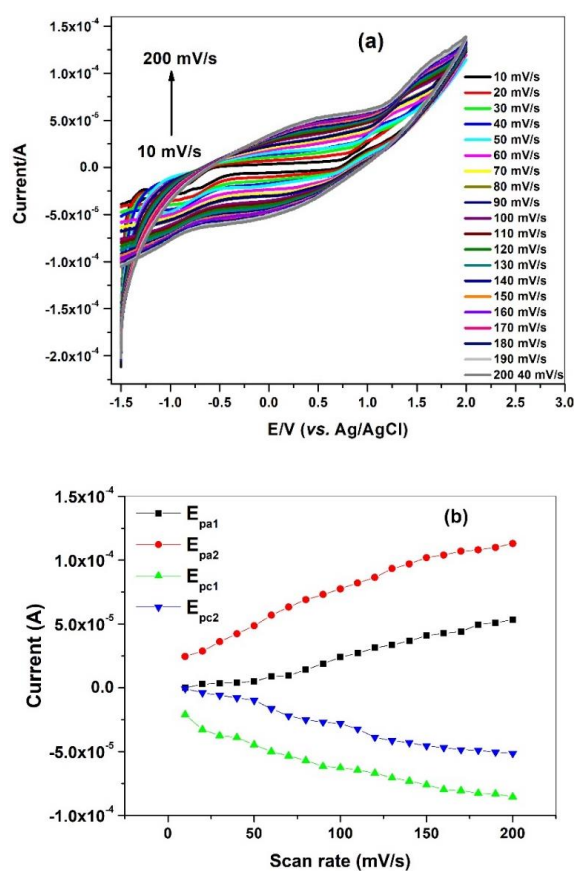

Figure 7. (**a**) Effect of the scan rate using a wide scan range, from 10 to 200 mV/s, (**b**) Effect of scan rate on the anodic and cathodic peak currents for **compound 4**.

3.5. Infrared Spectral Study

The infrared spectra of **compound 4** in both powder and thin-film forms are displayed in Figure 8. The synthesized **compound 4** molecules had several distinguished vibrational modes on the infrared spectrum. These bands were summarized as: (i) *O–H vibrations*, where the O–H phenolic group had two characteristic bands at 3414, 1452, and 1358 cm^{-1} due to stretching vibration motion, in-plane, and out-of-plane bending vibrations, and the out-of-plane deformation band was observed at 689 cm^{-1}; (ii) *N–H vibrations*, where the two bands observed at 3307 and 3199 cm^{-1} were assigned to asymmetric and symmetric motions of the N–H band; (iii) *C=O vibrations*, where the ν(C=O) of the cyclic ester group appeared as a very strong band at 1736 cm^{-1}, while the ν(C=N) of the 1,2,4-triazine moiety appeared as a medium-strong band at 1608 cm^{-1}; (iv) *C=C vibrations*, where the presence at 1494 cm^{-1} of a medium-strong intensity band was attributed to the C=C stretching mode, while the bending profile of such NH groups was exhibited at 1533 cm^{-1}, and the stretching profile of the C=S band appeared at 897 cm^{-1}; (v) *C–O vibrations*, where the medium-strong intensity band observed at 1290 cm^{-1} corresponded to the ν(C–O) vibrations; and (vi) *C–C and C–N vibrations*, where the medium intensity bands observed at 1217, 1173, 1106, and 1027 cm^{-1} corresponded to ν(C–C) vibrations. The FTIR spectra of **compound 4** in thin-film form showed good chemical and thermal stability up to 473 K.
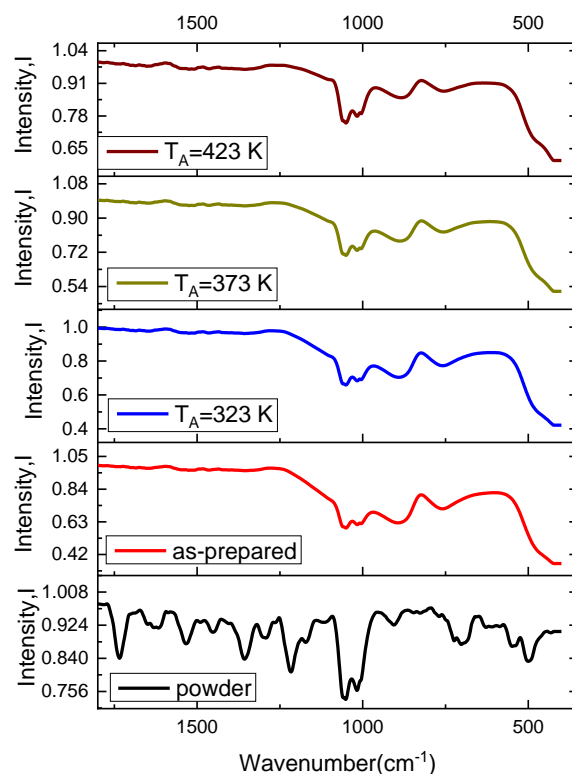

Figure 8. Infrared spectra of powder, as-deposited thin film, and annealed film (at 323K, 373K, and 423 K for 3 h in air) of **compound 4**.

3.6. X-ray Analysis

Figure 9 shows the XRD pattern of **compound 4**. The Rietveld method and Fullprof Suite program (2020) were used to find the refinement lattice parameters. The geometrical structure was drawn using VESTA-win 64 software. It was found that **compound 4** has a triclinic crystal structure with lattice parameters of a = 4.03416 Å, b = 13.73010 Å, c = 16.00670 Å, α = 113.4230°, β= 94.4060°, and γ= 93.0050° with space group (P-1) and a unit-cell volume of 807.795512 Å^3. An amorphous nature was observed for both as-deposited and annealed thin films.
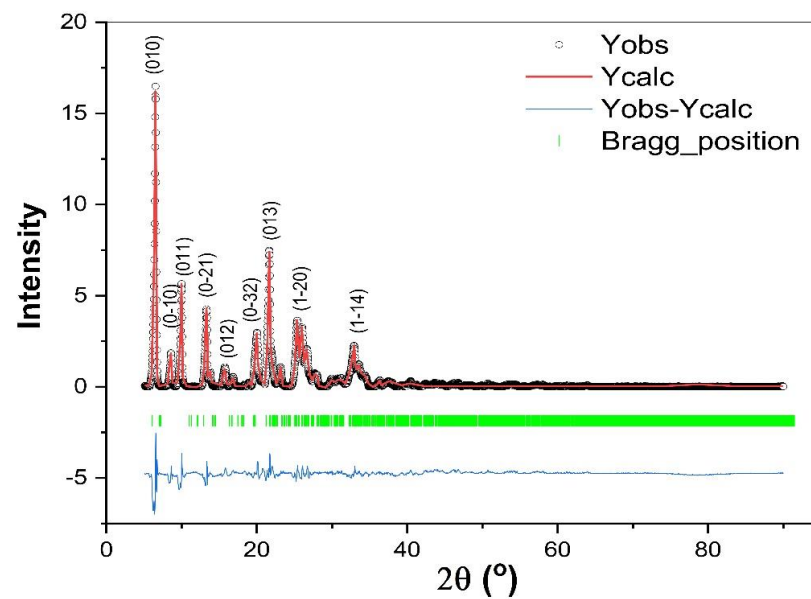
Figure 9. X-ray diffraction of **compound 4**. The inset figure shows X-ray diffraction (Y_{obs}) and the refined diffraction pattern (Y_{calc}) using the Rietveld method.

3.7. FESEM Analysis

The surface morphologies of the as-deposited and annealed **compound 4** thin films are shown in Figure 10a,b. All the thin films were characterized by homogeneous and uniform surface morphology. It can be observed from Figure 10a,b that the average value of the particle size for the as-deposited film increased with increasing temperature, which was due to the improvement in the crystallinity of the annealed film at 423 K for 3 h.
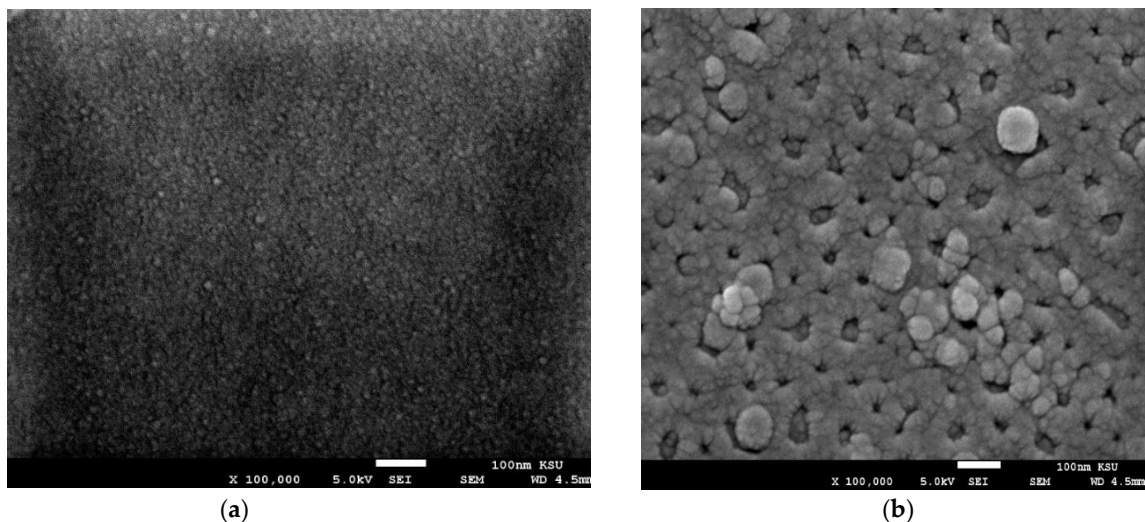

(**a**)　　　　　　　　　　　　　　　　　　　　　　　　　(**b**)

Figure 10. FESEM images of (**a**) as-deposited and (**b**) annealed **compound 4** thin films. The magnification is 100,000×, and the bar scale is 100 nm. The focal length of the objective lens is WD = 4.5 nm.

3.8. UV-Vis-NIR Spectroscopic Studies

The inset in Figure 11 shows the diffuse reflectance spectra (R_d) of **compound 4** in powder form. The diffuse reflectance spectra of inhomogeneous media can be discussed according to the Kubelka–Munk (K–M) function [48–50]:

$$F(R_d) \propto \alpha(h\nu) \propto \frac{(h\nu - E_g)^2}{h\vartheta} \tag{8}$$

where $F(R_d)$ is the Kubelka–Munk function, and α is the absorption coefficient of the organic powder. Figure 11 shows $(F(R_d)h\nu)^{1/2}$ versus ($h\nu$) for **compound 4**. The estimated values of the optical band transitions were found to be 2.07 eV and 2.67 eV. Altalhi et al. [48] estimated the optical band transitions of 4-amino-3-mercapto-6-(2-(2-thienyl)vinyl)-1,2,4-triazin-5(4H)-one donor as 2.72 eV.
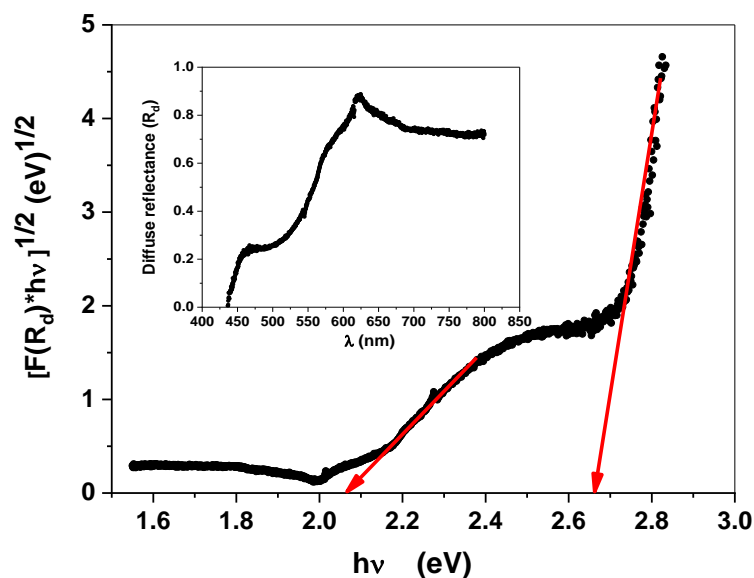

Figure 11. The relation between $[F(Rd)h\nu]^{1/2}$ versus ($h\nu$) of powder-form **compound 4**. The inset figure shows DRS spectra.

Figure 12 shows the T and R spectra of **compound 4**. It was observed that the values of the sharp band edge of transmittance for all the films were similar and not affected by the annealing temperatures. It is clear that all the thin films were transparent over the Vis-NIR spectral region. Also, the reflectance spectra slightly increased due to annealing in the transparent region.
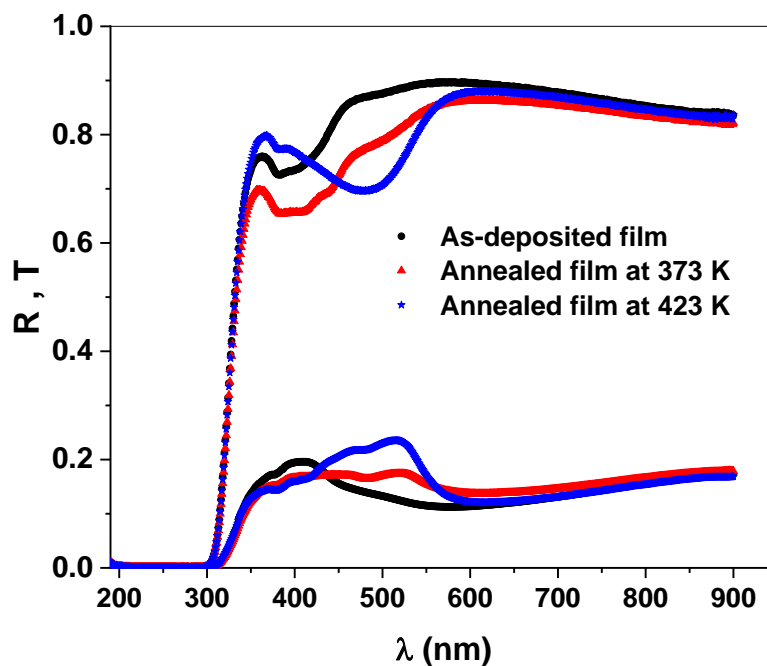

Figure 12. Optical transmittance (T) and reflectance (R) of **compound 4** thin films.

The absorption coefficient spectra (α) of the **compound 4** thin films are shown in Figure 13. It was realized that the absorption peak centered at 3.22 shifted to 2.52 eV due to annealing at 423 K. The annealing temperature slightly affected the sharp absorption edge of **compound 4.**
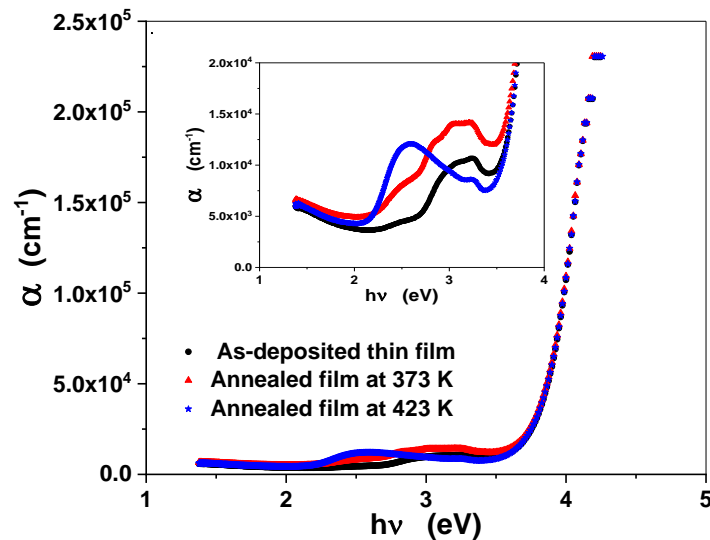

Figure 13. Plot of α versus photon energy for **compound 4** thin films.

The optical band transitions of **compound 4** thin films were estimated by using the relation for indirect optical transitions [48,51]:

$$(\alpha h\upsilon)^{\frac{1}{2}} = G\left(h\upsilon - E_g^{ind} \pm E_{phonon}\right) \tag{9}$$

where G is the probability parameter for the transition. Figure 14 shows the indirect optical band gap determined by plotting $(\alpha h\upsilon)^{\frac{1}{2}}$ versus ($h\upsilon$) for **compound 4** thin films. The value of the indirect optical transitions obtained from the graph was $E_g^{ind} = 3.6\ V$ for both the as-deposited and annealed thin films.
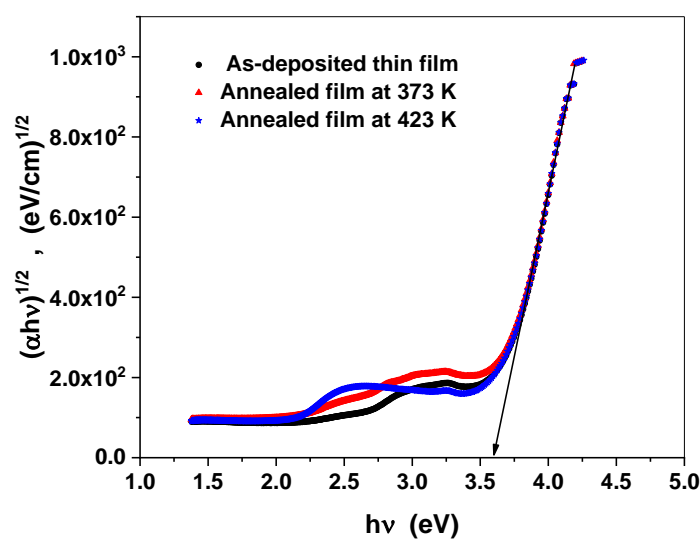

Figure 14. Plot of $(\alpha h\vartheta)^{1/2}$ versus photon energy for **compound 4** thin films.

At an excitation wavelength of 250 nm, normalized PL spectra for **compound 4** thin films are shown in Figure 15a,b. For the as-deposited film, there were two PL emission peaks centered at 473 and 490 nm with a shoulder at 422 nm. For the annealed film, there

were five PL emission peaks centered at 274, 416, 439, 464, and 707 nm with a shoulder at 548 nm. The interband transitions of π^*–π or π^*–n from the LUMO to the HOMO are commonly used to understand the observed PL emissions peaks [52].
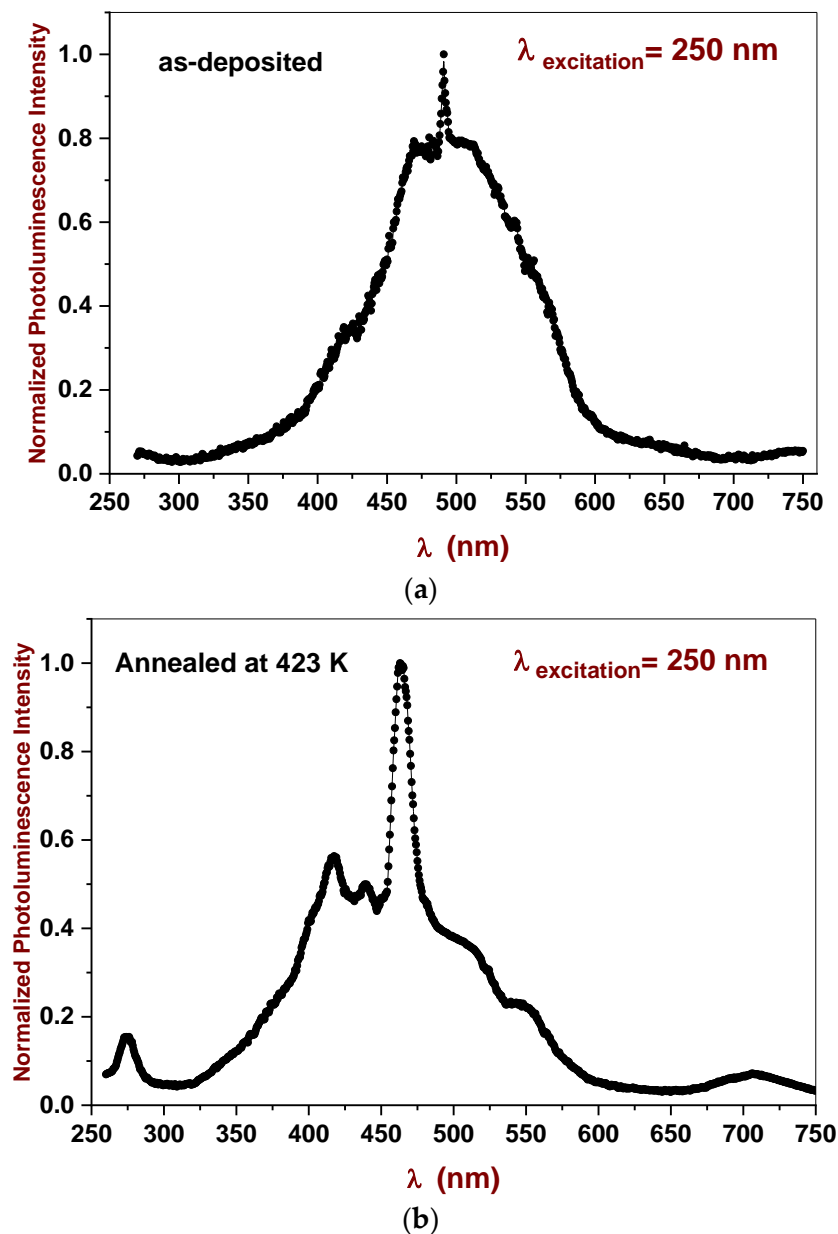

Figure 15. Normalized PL spectra of (**a**) as-deposited and (**b**) annealed **compound 4** thin films.

Figure 16 shows the spectral dependence of the real part of the refractive index (n) of **compound 4** thin films. It was observed that the values of n in the transparent region decreased gradually and steadily in the wavelength range of 550–900 nm. In addition, at $\lambda = 900$ nm, it was observed that the refractive index were slightly increased by annealing, from 1.91 at room temperature to 2.15 after annealing at 423 K for 3 h. The peak centered at 406 nm shifted to 512 nm after annealing at 423 K for 3 h. The increase in the refractive index (n) can be attributed to an improvement in the crystallinity of the films, as confirmed by FESEM.
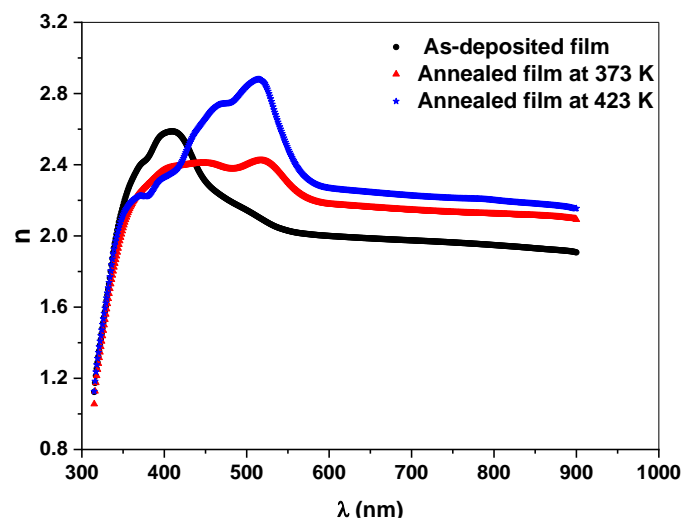
Figure 16. The spectral dependence of the real part of the refractive index of **compound 4** thin films.

The optical dispersion parameters of the organic material were real candidates for optoelectronic devices. To obtain the dispersion energy (E_d), the single oscillator energy (E_o) and the infinite frequency dielectric constant (ε_∞), the real part of the refractive index in the transparent region (normal dispersion behavior), were analyzed using a single oscillator model [53–55]:

$$\frac{1}{n^2 - 1} = \frac{E_0}{E_d} - \frac{1}{E_o E_d}(h\nu)^2 \tag{10}$$

A plot of $(n^2-1)^{-1}$ versus $(h\nu)^2$ for **compound 4** thin films is shown in Figure 17.
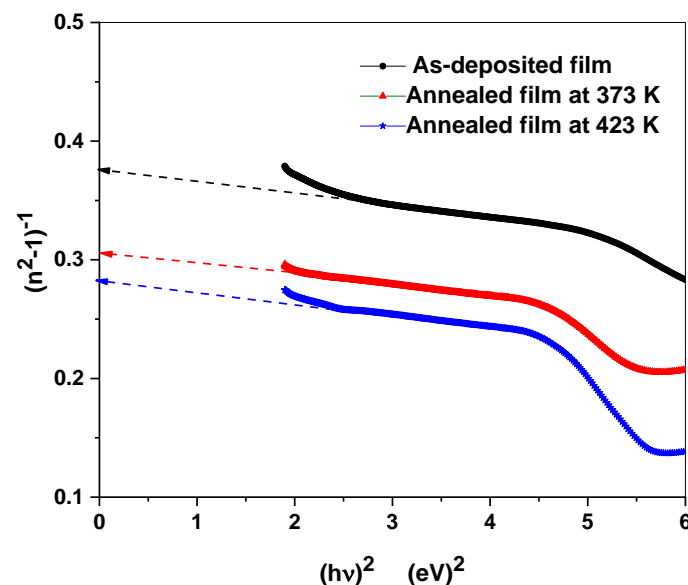

Figure 17. Plot of $(n^2-1)^{-1}$ films versus $(h\nu)^2$ for **compound 4** thin films.

In addition, the link between the lattice dielectric constant ε_L $(= n^2)$ and λ^2 at longer wavelengths was expressed according to the following relation [56–58]:

$$\varepsilon_1 = n^2 = \varepsilon_L - \frac{e^2 N}{4\pi^2 \varepsilon_o m^* c^2}\lambda^2, \tag{11}$$

where ε_o is the permittivity of free space, e is the electronic charge, c is the velocity of light, and N/m^* is the ratio of free charge carrier concentration to the effective mass.

Figure 18 shows the plot between n^2 and λ^2 of **compound 4** thin films. ε_L and N/m^* were calculated from analysis of the linear part at longer wavelengths. The changes in the estimated values of the optical dispersion parameters with annealing were attributed to improvement in crystallinity of the **compound 4** thin film. The optical dispersion parameter values are tabulated in Table 2.
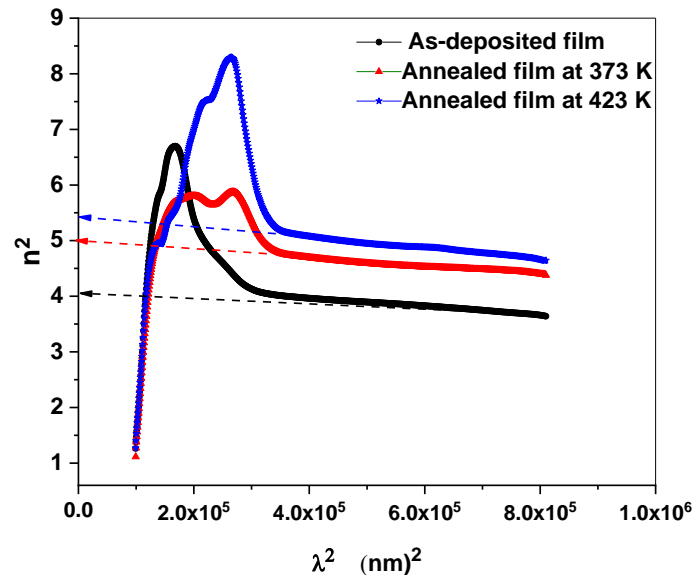

Figure 18. Plot of n^2 versus λ^2 for **compound 4** organic thin films.

Table 2. Optical dispersion parameters of **compound 4** thin films.

Compound 4 Thin Films	E_o (eV)	E_d (eV)	ε_∞	ε_L	$\frac{N}{m^*}(\mathbf{10^{45}})$ $(g^{-1}cm^{-3})$
As-deposited	6.11	16.25	3.66	4.27	91
Annealed at 373 K	5.95	16.28	3.73	4.29	70
Annealed at 423 K	5.27	20.43	4.51	4.53	114.3
Ref [48] for as-deposited film	5.8	12.3	3.12	3.15	1.56
Ref [48] for annealed film at 373 K	5.85	11.89	3.00	3.04	3.73

The dark DC electrical conductivity, σ_{dc} against 1000/T (during heating and cooling treatments), for the as-deposited **compound 4** thin film in the temperature range of 298–380 K is displayed in Figure 19. The cooling run showed lower conductivity than the heating run due to the removal of the absorbed and adsorbed gases on the surface of the organic thin film [59,60]. In addition, the figure shows that the electrical conduction was through a thermally activated process. The activation energy (ΔE) was estimated via a usual Arrhenius relation [61]:

$$\sigma_{dc} = \sigma_0 \exp\left(-\frac{\Delta E}{k_B T}\right) \tag{12}$$

where k_B is the Boltzmann constant, and At T → 0 $\sigma_0 = \sigma_{dc}$ and ΔE are the thermal activation energies of the free charge carriers through the **compound 4** thin film. The calculated value of ΔE was found to be 0.82 eV for both the heating and cooling treatments.
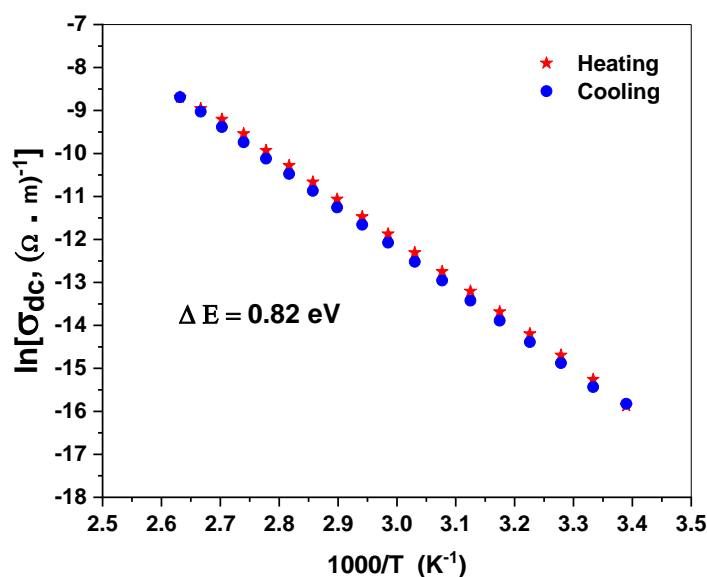
Figure 19. Dependence of $\ln(\sigma_{dc})$ on inverse temperature for **compound 4** thin film.

4. Conclusions

The chemical structure of synthesized 5-(5-Bromo-2-hydroxybenzylidene)-6-oxo-3-phenyl-5,6-dihydro-1,2,4-triazine-2(1H)-carbothioamide (4) was confirmed by spectroscopic techniques (FTIR, ^{1}H-NMR, and ^{13}C-NMR). The kinetic parameters of **compound 4** such as ΔS^*, ΔH^*, and ΔG^* were estimated using the Coats–Redfern equation. The onsets of oxidation $E_{(onset\ oxidation)}$ and reduction $E_{(onset\ reduction)}$ peaks were −0.76 V and +0.92 V, respectively. The calculated HOMO, LUMO, and the band gap ($E_g^{electrochemical}$) were −3.64 eV, −5.32 eV, and 1.68 eV, respectively. The FTIR spectra of **compound 4** in thin-film form showed good chemical and thermal stability up to 473 K. XRD analysis of **compound 4** in powder form was investigated using the Fullprof Suite program. The structural parameter results indicated that **compound 4** has a triclinic crystal structure with lattice parameters of a = 4.03416 Å, b = 13.73010 Å, c = 16.00670 Å, α = 113.4230°, β = 94.4060°, and γ = 93.0050° with space group (P -1) and a unit-cell volume of 807.795512 Å^3. In addition, it was found that the as-deposited and annealed films were characterized by an amorphous nature. The FESEM results showed that the average values of particle size increased with increasing temperature, correlating well with the improvement in the crystallinity of the annealed film. The estimated values of the allowed indirect optical band transitions were found to be 2.07 *e*V and 2.67 *e*V from optically diffused reflectance of **compound 4** in powder form. The value of the optical transition was found to be $E_g^{ind} = 3.6\ V$. The values of sharp band edge transmittance of all the films were similar and not affected by the annealing temperatures. The as-deposited film showed two PL emission peaks centered at wavelengths of 473 nm and 490 nm with a shoulder at 422 nm, whereas the annealed film showed five PL emission peaks centered at wavelengths 274 nm, 416 nm, 439 nm, 464 nm, and 707 nm with a shoulder at 548 nm. The increase in the refractive index with increasing temperatures was attributed to improvement in the crystallinity of the films. The calculated value of ΔE for the DC electrical conductivity was found to be 0.82 eV for both the heating and cooling treatments. The spectroscopic and physicochemical parameters of the synthesized **compound 4** demonstrated their future appropriate action in advanced photonic applications. Novel organic molecules with highly reactive chromophores and ultra-optical activity, as a response to the demand for materials, can be used in various fields, such as modern applications, improving human life, and environmental remediation.

References

1. Yu, H.; He, Y.; Wu, Y.; He, Y.; He, C.; Meng, H. Thermally stable organic thin film transistors based on 2-(anthracen-2-yl)tetracene. *Org. Electron.* **2020**, *85*, 105787. [CrossRef]
2. Lia, J.-N.; Wu, Y.; Zhang, X.; Zeng, D.; Luo, Y.; Duan, X.; Gao, X.; Cai, P.; Zhang, Q.; Zhang, J.; et al. A new fluorinated pyran-bridged A-D-A type small molecular acceptor for organic solar cells. *Dye. Pigment.* **2020**, *175*, 108165. [CrossRef]
3. Madrid-Úsuga, D.; Mora-León, A.G.; Cabrera-Espinoza, A.M.; Insuasty, B.; Ortiza, A. Theoretical characterization of photoactive molecular systems based on BODIPY-derivatives for the design of organic solar cells. *Comput. Theor. Chem.* **2021**, *1197*, 113165. [CrossRef]
4. Yen, Y.-S.; Hsu, J.-L.; Ni, J.-S.; Lin, J.T. Influence of various dithienoheterocycles as conjugated linker in Naphtho [2,3-d] [1,2,3]triazole-based organic dyes for dye-sensitized solar cells. *Dye. Pigment.* **2021**, *188*, 109220. [CrossRef]
5. Bibi, S.; Khera, R.A.; Farhat, A.; Iqbal, J. Triphenylamine based donor-acceptor-donor type small molecules for organic solar cells. *Comput. Theor. Chem.* **2021**, *1198*, 113176. [CrossRef]
6. Sharif, A.; Jabeen, S.; Iqbal, S.; Iqbal, J. Tuning the optoelectronic properties of dibenzochrysene (DBC) based small molecules for organic solar cells. *Mater. Sci. Semicond. Process.* **2021**, *127*, 105689. [CrossRef]
7. D.Branowska, E.; Olender, W.; Wysocki, Z.; Karczmarzyk, I.; Bancerz, P.; Ledwon, M.; Lapkowski, B.; Mirosław, Z.; Urbańczyk-Lipkowska, P. Kalicki, Synthesis and electrochemical characterization of oligothiophenes with 1,2,4-triazine and 5,5/ -bi-1,2,4-triazine as strong electron acceptor units. *Electrochim. Acta* **2016**, *214*, 19.
8. Sakr, M.E.M.; Kana, M.T.H.A.; Elwahy, A.H.M.; El-Daly, S.A.; Ebeid, E.M. Novel far UV-Vis absorbing bis(dihydrophenanthro[9,10-e][1,2,4] triazine) derivative dyes: Synthesis, optical, photophysical and solvatochromic properties. *J. Mol. Struct.* **2020**, *1206*, 127690. [CrossRef]
9. Grimsdale, A.C.; Chan, K.L.; Martin, R.E.; Jokisz, P.G.; Holmes, A.B. Synthesis of light-emitting conjugated polymers for applications in electroluminescent devices. *Chem. Rev.* **2009**, *109*, 897. [CrossRef]
10. Braga, D.; Horowitz, G. High-performance organic field-effect transistors. *Adv. Mater.* **2009**, *21*, 1473. [CrossRef]
11. Radford, R.J.; Chyan, W.; Lippard, S.J. Peptide-based targeting of fluorescent zinc sensors to the plasma membrane of live cells. *Chem. Sci.* **2013**, *4*, 3080–3084. [CrossRef]
12. Facchetti, A. π-Conjugated polymers for organic electronics and photovoltaic cell applications. *Chem. Mater.* **2011**, *23*, 733. [CrossRef]
13. Reineke, S.; Lindner, F.; Schwartz, G.; Seidler, N.; Walzer, K.; Lussem, B.; Leo, K. White organic light-emitting diodes with fluorescent tube efficiency. *Nature* **2009**, *459*, 234. [CrossRef] [PubMed]
14. Xiao, L.X.; Chen, Z.J.; Qu, B.; Luo, J.X.; Kong, S.; Gong, Q.H.; Kido, J.J. Full phosphorescent white-light organic light-emitting diodes with improved color stability and efficiency by fine tuning primary emission contributions. *Adv. Mater.* **2011**, *23*, 926. [CrossRef] [PubMed]
15. Zhang, W.; Zhu, C.; Huang, Z.; Gong, C.; Tang, Q.; Fu, X. Electrochromic 2,4,6-triphenyl-1,3,5-triazine based esters with electron donor-acceptor structure. *Org. Electron.* **2018**, *67*, 302–310. [CrossRef]
16. Wu, N.; Ma, L.; Zhao, S.; Xiao, D. Novel triazine-centered viologen analogues for dual-band electrochromic devices. *Sol. Energy Mater. Sol. Cells* **2019**, *195*, 114–121. [CrossRef]
17. Data, P.; Zassowski, P.; Lapkowski, M.; Grazulevicius, J.V.; Kukhta, N.A.; Reghu, R.R. Electrochromic behavior of triazine based ambipolar compound. *Electrochim. Acta* **2016**, *192*, 283–295. [CrossRef]
18. Zeng, W.D.; Cao, Y.M.; Bai, Y.; Wang, Y.H.; Shi, Y.S.; Zhang, M.; Wang, F.F.; Pan, C.Y.; Wang, P. Efficient Dye-Sensitized Solar Cells with an Organic Photosensitizer Featuring Orderly Conjugated Ethylenedioxythiophene and Dithienosilole Blocks. *Chem. Mater.* **2010**, *22*, 1915. [CrossRef]
19. Arias, A.C.; MacKenzie, J.D.; McCulloch, I.; Rivnay, J.; Salleo, A. Materials and applications for large area electronics: Solution-based approaches. *Chem. Rev.* **2010**, *110*, 3. [CrossRef]

20. Rahulan, K.M.; Balamurugan, S.; Meena, K.; Yeap, G.Y.; Kanakam, C.C. Synthesis and nonlinear optical absorption of novel chalcone derivative compounds. *Opt. Laser Technol.* **2014**, *56*, 142–145. [CrossRef]

21. Huang, D.-C.; Wu, J.-T.; Fan, Y.-Z.; Liou, G.-S. Preparation and optoelectronic behaviours of novel electrochromic devices based on triphenylamine-containing ambipolar materials. J. *Mater. Chem. C* **2017**, *5*, 9370–9375. [CrossRef]

22. Lv, X.; Li, W.; Ouyang, M.; Zhang, Y.; Wright, D.S.; Zhang, C. Polymeric electrochromic materials with donor–acceptor structures. J. *Mater. Chem. C* **2017**, *5*, 12–28. [CrossRef]

23. Signore, G.; Nifosií, R.; Albertazzi, L.; Storti, B.; Bizzarri, R. Polarity-Sensitive Coumarins Tailored to Live Cell Imaging. *J. Am. Chem. Soc.* **2010**, *132*, 1276–1288. [CrossRef] [PubMed]

24. Cheng, Y.-J.; Yang, S.-H.; Hsu, C.-S. Synthesis of Conjugated Polymers for Organic Solar Cell Applications. *Chem. Rev.* **2009**, *109*, 5868–5923. [CrossRef]

25. Thirumurugan, P.; Perumal, P.T. The synthesis and photophysical studies of pyridinyl-1,2,4-triazine derivatives and use as a fluorescent sensor for ferric salts. *Dye. Pigment.* **2011**, *88*, 403–412. [CrossRef]

26. Guo, Z.-H.; Jin, Z.-X.; Wang, J.-Y.; Pei, J. A donor–acceptor–donor conjugated molecule: Twist intramolecular charge transfer and piezochromic luminescent properties. *Chem. Commun.* **2014**, *50*, 6088–6090. [CrossRef]

27. Richard, A.; Klenklera, H.A.; Tranc, A.; Popovic, D.Z.; Xu, G. High electron mobility triazine for lower driving voltage and higher efficiency organic light emitting devices. *Org. Elect.* **2008**, *9*, 285.

28. Zinatloo-Ajabshir, S.; Emsaki, M.; Hosseinzadeh, G. Innovative construction of a novel lanthanide cerate nanostructured photocatalyst for efficient treatment of contaminated water under sunlight. *J. Colloid Interface Sci.* **2022**, *619*, 1–14. [CrossRef]

29. Zinatloo-Ajabshir, S.; Morassaei, M.S.; Salavati-Niasari, M. Eco-friendly synthesis of $Nd_2Sn_2O_7$–based nanostructure materials using grape juice as green fuel as photocatalyst for the degradation of erythrosine. *Compos. Part B* **2019**, *167*, 643–653. [CrossRef]

30. Mahdavi, K.; Zinatloo-Ajabshir, S.; Yousif, Q.A.; Salavati-Niasari, M. Enhanced photocatalytic degradation of toxic contaminants using Dy_2O_3-SiO_2 ceramic nanostructured materials fabricated by a new, simple and rapid sonochemical approach. *Ultrason. Sonochem.* **2022**, *82*, 105892. [CrossRef]

31. Tabatabaeinejad, S.M.; Zinatloo-Ajabshir, S.; Amiric, O.; Salavati-Niasari, M. Magnetic $Lu_2Cu_2O_5$-based ceramic nanostructured materials fabricated by a simple and green approach for an effective photocatalytic degradation of organic contamination. *RSC Adv.* **2021**, *11*, 40100–40111. [CrossRef] [PubMed]

32. Zinatloo-Ajabshir, S.; Salavati-Niasari, M. Preparation of nanocrystalline cubic ZrO_2 with different shapes via a simple precipitation approach. *J. Mater. Sci. Mater. Electron.* **2016**, *27*, 3918–3928. [CrossRef]

33. Ghavidast, A.; Mahmoodi, N.O. A comparative study of the photochromic compounds incorporated on the surface of nanoparticles. *J. Mol. Liq.* **2016**, *216*, 552–564. [CrossRef]

34. Zinatloo-Ajabshir, S.; Morassaei, M.S.; Salavati-Niasari, M. Facile fabrication of $Dy_2Sn_2O_7$-SnO_2 nanocomposites as an effective photocatalyst for degradation and removal of organic contaminants. *J. Colloid Interface Sci.* **2017**, *497*, 298–308. [CrossRef]

35. El-Nahass, M.M.; Metwally, H.S.; El-Sayed, H.E.A.; Hassanien, A.M. Electrical and photovoltaic properties of FeTPPCl/p-Si heterojunction. *Synth. Met.* **2011**, *161*, 2253–2258. [CrossRef]

36. Alrooqi, A.; Al-Amshany, Z.M.; Al-Harbi, L.M.; Altalhi, T.A.; Refat, M.S.; Hassanien, A.M.; Atta, A.A. Impact of Charge Transfer Complex on the Dielectric Relaxation Processes in Poly(methyl methacrylate) Polymer. *Molecules* **2022**, *27*, 1993. [CrossRef]

37. Hassanien, A.M.; Atta, A.; Ward, A.A.; Ahmed, E.M.A.; Alsubaie, A.; El-Nahass, M.; Altalhi, T. Investigation of structural, electrical and optical properties of chitosan/fullerene composites. *Mater. Res. Express* **2019**, *6*, 125304. [CrossRef]

38. Zinatloo-Ajabshir, S.; Morassaei, M.S.; Amiri, O.; Salavati-Niasari, M. Green synthesis of dysprosium stannate nanoparticles using Ficus carica extract as photocatalyst for the degradation of organic pollutants under visible irradiation. *Ceram. Int.* **2019**, *46*, 6095–6107. [CrossRef]

39. Zinatloo-Ajabshir, S.; Mousavi-Kamazani, M. Recent advances in nanostructured Sn-Ln mixed-metal oxides as sunlight-activated nanophotocatalyst for high-efficient removal of environmental pollutants. *Ceram. Int.* **2021**, *47*, 23702–23724. [CrossRef]

40. Zinatloo-Ajabshir, S.; Salavati-Niasari, M.; Zinatloo-Ajabshir, Z. $Nd_2Zr_2O_7$-Nd_2O_3 nanocomposites: New facilesynthesis, characterization and investigation of photocatalytic behaviour. *Mater. Lett.* **2016**, *180*, 27–30. [CrossRef]

41. Etemadi, H.; Afsharkia, S.; Zinatloo-Ajabshir, S.; Shokri, E. Effect of alumina nanoparticles on the antifouling properties of polycarbonate-polyurethane blend ultrafiltration membrane for water treatment. *Polym Eng Sci.* **2021**, *61*, 2364–2375. [CrossRef]

42. Nemytov, A.I.; Utepova, I.A.; Kiskin, M.A.; Efimov, N.N.; Fedin, M.V.; Eremenko, I.L.; Musikhina, A.A.; Slepukhin, P.A.; Chupakhin, O.N. Synthesis, structure and magnetic properties of binuclear 3d-metal complexes of new 3-(2-pyridyl)-6-phenyl-1,2,4-triazine derivative. *Polyhedron* **2020**, *193*, 114901. [CrossRef]

43. Saloutina, L.; Zapevalov, A.Y.; Kodess, M.; Slepukhin, P.; Ganebnykh, I.; Saloutin, V.; Chupakhin, O. Trifluoromethyl–containing 1,2,4-triazines. Synthesis on the base of perfluorobiacetyl and reactions with thiosemicarbazide and thiourea. *J. Fluor. Chem.* **2019**, *227*, 109362. [CrossRef]

44. Coats, A.W.; Redfern, J.P. Kinetic Parameters from Thermogravimetric Data. *Nature* **1964**, *201*, 68–69. [CrossRef]

45. Dodd, J.W.; Tonge, K.H. *Thermal Methods*; John Wiley& Sons: New York, NY, USA; London, UK, 1987.

46. Kong, Z.; Liu, D.; He, J.; Wang, X. Electrode buffer layers producing high performance nonvolatile organic write-once-read-many-times memory devices. *RSC Adv.* **2017**, *7*, 13171–13176. [CrossRef]

47. Li, J.; Zhong, H.; Liu, H.; Zhai, T.; Wang, X.; Liao, M.; Bando, Y.; Liua, R.; Zou, B. One dimensional ternary Cu–Bi–S based semiconductor nanowires: Synthesis, optical and electrical properties. *J. Mater. Chem.* **2012**, *22*, 17813–17819. [CrossRef]

48. Altalhi, T.; Gobouri, A.A.; Refat, M.S.; El-Nahass, M.M.; Hassanien, A.M.; Atta, A.A.; Saad, H.A.; Alhazaa, A.N. Structural, electrochemical and optical properties of 1,2,4-triazine derivative. *Appl. Phys. A* **2020**, *126*, 815. [CrossRef]

49. Philips-Invernizzi, B.; Dupont, D.; Caze, C. Bibliographical review for reflectance of diffusing media. *Opt. Eng.* **2001**, *40*, 1082–1092. [CrossRef]

50. Mishra, V.; Warshi, M.K.; Sati, A.; Kumar, A.; Mishra, V.; Sagdeo, A.; Kumar, R.; Sagdeo, P.R. Diffuse reflectance spectroscopy: An effective tool to probe the defect states in wide band gap semiconducting materials. *Mater. Sci. Semicond. Process.* **2018**, *86*, 151–156. [CrossRef]

51. Altalhi, T.; Gobouri, A.A.; Refat, M.S.; El-Nahass, M.M.; Hassanien, A.M.; Atta, A.A.; al Otaibi, S.; Kamal, A.M. Optical spectroscopic studies on poly(methyl methacrylate) doped by charge transfer complex. *Opt. Mater.* **2021**, *117*, 111152. [CrossRef]

52. Kafle, B.P. Chemical Analysis and Material Characterization by Spectrophotometry. Elsevier: Amsterdam, The Netherlands, 2020; pp. 269–296.

53. Wemple, S.H.; DiDomenico Jr., M. Behavior of the Electronic Dielectric Constant in Covalent and Ionic Materials. *Phys. Rev. B* **1971**, *3*, 1338. [CrossRef]

54. Wemple, S.H. Refractive-Index Behavior of Amorphous Semiconductors and Glasses. *Phys. Rev. B* **1973**, *7*, 3767–3777. [CrossRef]

55. El-Nahass, M.M.; Zayed, H.A.; Elgarhy, E.E.; Hassanien, A.M. Effect of γ- irradiation on structural, optical and electrical properties of thermally evaporated iron (III) chloride tetraphenylporphyrin thin films, Radiat. *Phys. Chem.* **2017**, *139*, 173–178.

56. Edward Palik, D. *Handbook of Optical Constants of Solids*; Academic Press: New York, NY, USA, 1985; p. 265.

57. El-Nahass, M.; El-Deeb, A.; Metwally, H.; Hassanien, A. Influence of annealing on the optical properties of 5,10,15,20-tetraphenyl-21H, 23H-porphine iron (III) chloride thin films. *Mater. Chem. Phys.* **2011**, *125*, 247–251. [CrossRef]

58. El-Nahass, M.; El-Deeb, A.; Metwally, H.; El-Sayed, H.; Hassanien, A. Influence of X-ray irradiation on the optical properties of iron (III) chloride tetraphenylporphyrin thin films. *Solid State Sci.* **2010**, *12*, 552–557. [CrossRef]

59. Leontie, L.; Druta, I.; Danac, R.; Prelipceanu, M.; Rusu, G.I. Electrical properties of some new high resistivity organic semiconductors in thin films. *Prog. Org. Coat.* **2005**, *54*, 175–181. [CrossRef]

60. Hassanien, A.M. Surface topology, optical spectroscopic and electrical studies on boron subphthalocyanine chloride thin films. *J. Dispers. Sci. Technol.* **2021**, 1–8. [CrossRef]

61. Mott, N.F.; Davis, E.A. *Electronic Processes in Non-Crystalline Materials*, 2nd ed.; Clarendon Press: Oxford, UK, 1979.